Parametric dislocation dynamics: A thermodynamics-based approach to investigations of mesoscopic plastic deformation

N. M. Ghoniem, S.-H. Tong, and L. Z. Sun
Mechanical and Aerospace Engineering Department, University of California, Los Angeles, California 90095-1597
(Received 16 July 1999)

A thermodynamics-based variational method is developed to establish the equations of motion for three-dimensional (3D) interacting dislocation loops. The approach is appropriate for investigations of plastic deformation at the mesoscopic scale by direct numerical simulations. A fast sum technique for determination of elastic field variables of dislocation ensembles is utilized to calculate forces acting on generalized coordinates of arbitrarily curved loop segments. Each dislocation segment is represented by a parametric space curve of specified shape functions and associated degrees of freedom. Kinetic equations for the time evolution of generalized coordinates are derived for general 3D climb/glide motion of curved dislocation loops. It is shown that the evolution equations for the position (**P**), tangent (**T**), and normal (**N**) vectors at segment nodes are sufficient to describe general 3D dislocation motion. When crystal structure constraints are invoked, only two degrees of freedom per node are adequate for constrained glide motion. A selected number of applications are given for: (1) adaptive node generation on interacting segments, (2) variable time-step determination for integration of the equations of motion, (3) dislocation generation by the Frank-Read mechanism in fcc, bcc, and dc crystals, (4) loop-loop deformation and interaction, and (5) formation of dislocation junctions.

I. INTRODUCTION

A fundamental description of plastic deformation is now actively pursued, where dislocations play a key role as basic elements of metal plasticity. Although continuum plasticity models are extensively used in engineering practice, their validity is limited to the underlying database. The reliability of continuum plasticity descriptions is dependent on the accuracy of experimental data. Under complex loading situations, however, the database is often hard to establish. Moreover, the lack of a characteristic length scale in continuum plasticity makes it difficult to predict the occurance of critical localized deformation zones. Although homogenization methods have played a significant role in determining the elastic properties of new materials from their constituents (e.g., composite materials), the same methods have failed to describe plasticity. It is widely appreciated that plastic strain is fundamentally heterogenous, displaying high strains concentrated in small material volumes, with virtually undeformed regions in between. Experimental observations consistently show that plastic deformation is internally heterogeneous at a number of length scales.[1–4] Depending on the deformation mode, heterogeneous dislocation structures appear with definitive wavelengths. It is common to observe persistent slip bands, shear bands, dislocation pile ups, dislocation cells, and subgrains. However, a satisfactory description of realistic dislocation patterning and strain localization has been rather elusive. Attempts directed at this question have been based on statistical mechanics,[5–10] reaction-diffusion dynamics,[11–13] and the theory of phase transitions.[14] Much of the efforts represented by Refs. 5–14 have aimed at clarifying the fundamental origins of inhomogeneous plastic deformation.

A relatively recent approach to investigation of the fundamental nature of plastic deformation is based on direct numerical simulation of the interaction and motion of dislocations. This approach, which is commonly known as dislocation dynamics (DD), was first introduced for two-dimensional (2D) straight, infinitely long dislocation distributions,[15–27] and then later for complex 3D microstructure.[28–44] In DD simulations of plastic deformation, the computational effort per time step is proportional to the square of the number of interacting segments, because of the long-range stress field associated with dislocation lines. The computational requirements for 3D simulations of plastic deformation of even single crystals are thus very challenging. It is therefore advantageous to reduce the total number of equations of motion during such calculations. Pioneering 3D DD simulations of plasticity using straight segments are based on existing analytical solutions of the elastic field of pure screw and edge segments,[28–38] or segments of mixed character.[39–43] Zbib, Rhee, and Hirth[43] determined that the length of each straight segment is roughly limited to $\sim 50-200$ units of Burgers vector. Longer segments may have substantial force variations, thus limiting the usefulness of one single equation of motion for the entire segment. Singular forces and stresses arise at sharp intersection corners of straight segments, which result in divergence of the average force over the straight segment as its length is decreased. When the dislocation loop is discretized to only screw or edge components on a crystallographic lattice,[28–38] the accuracy of strong dislocation interactions is compromised because line curvatures are crudely calculated. In addition, motion of dislocation segments on a fixed lattice produces inherent limitations to the resolution of space and time events. Recently, Schwartz[40–42] developed an adaptive method to reduce the segment size when dislocation interactions become strong. Using a modified form of the Brown formula[45] for the self-force on a segment, the field divergence problem for very short segments was circumvented. For closely interacting dislocations, substantial curvature and

reconfiguration of dislocations occur during the formation of a junction, dipole, or other configurations.[42] However, the number of straight segments required to capture these processes is very large, because the segment size has to be reduced to a few Burgers vectors. Most of these difficulties arise from the linear segment approximation, the *differential* treatment of the equations of motion, and the accuracy of representing the self-force.

Dislocation loops in DD computer simulations are treated as dynamical systems, which can be described by the time dependence of specified coordinates. Obviously, if one attempts to solve the equations of dynamics for each atom within and surrounding the dislocation core, the number of equations is prohibitively large. On the other hand, if one knows that certain modes of motion for groups of atoms are closely linked, many equations can be *adiabatically* eliminated, as is now conventional in the treatment of dynamical systems. Thus, instead of developing equations for the motion of each atom, one can find a much smaller set of geometric *generalized coordinates*, which would adequately describe the dynamical behavior of an entire dislocation loop. In Lagrangian descriptions, a number of generalized coordinates, q_r, is selected, where the subscript r represents a specific *degree of freedom* (DOF) for the dynamical system. In a numerical computer simulation, however, the size of the system depends on available N_{DF}. Within the context of DD, one would expect that N_{DF} is relatively small in loops, which conform to specific crystallographic or mobility constraints, while N_{DF} can be somewhat large in situations where strong interactions, cross-slip, or similar processes take place. In general, it is not of interest to follow every wiggle and bump on dislocation lines, unless such details develop into full-fledged instabilities. For specific applications, however, we intend to reduce N_{DF} as much as reasonable for the description of the physical situation at hand.

Our plan here is to describe the equations of motion for generalized coordinates in much the same way as in Lagrangian mechanics. We will develop an *integral* equation of motion for each curved segment within the loop, regardless of dislocation loop shape complexity. For concreteness, we focus the current approach on dislocation line representation by parametric dislocation segments, similar to the finite element method. Thus, the equations of motion for the transport of atoms within the dislocation core should be consistent with the thermodynamics of irreversibility. A challenging prospect in such a description is the enormous topological complexity of materials containing dislocations. Dislocation lines assume complex shapes, particularly during heavy deformation and at high temperatures, where they execute truly 3D motion as a result of combined glide and climb forces. These dislocations can be highly curved because of their strong mutual interactions, externally applied stress fields, as well as other thermodynamic forces. It is apparent that whenever large curvature variations are expected, the accuracy of computing the dynamic shape of dislocation loops becomes critical.

The paper is organized as follows. First, irreversible thermodynamics of dislocation motion is presented in Sec. II, in which we discuss energy components and entropy production during loop motion. This leads to an integral form of the variation in Gibbs energy in Sec. III. A *weak* form of a variational procedure is pursued to formulate the equations of motion for the degrees of freedom based on the Galerkin approach. Computational *protocols*, which are used to handle close-range interactions are then discussed in Sec. IV. To help illustrate the computational procedure, a simple example is also given. Applications of the present method to dislocation motion under physical constraints, and to several problems of loop-loop interaction and dislocation generation in fcc, bcc, and diamond cubic (dc) Si crystals are given in Sec. V. Finally, conclusions and discussions follow in Sec. VI.

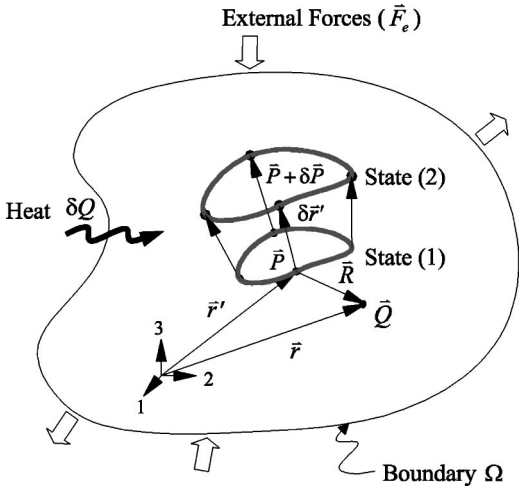

FIG. 1. Representation of loop motion in an infinitesimal transition, illustrating thermodynamic variables.

II. IRREVERSIBLE THERMODYNAMICS OF DISLOCATION MOTION

Consider a body in thermodynamic equilibrium, volume Ω, and its boundary $\mathcal{S}$, containing a dislocation loop in an initial position (1), as shown in Fig. 1. Under the influence of external mechanical forces ($\mathbf{F}_e$), and thermodynamic internal forces ($\mathbf{F}_i$), the dislocation loop will undergo a transition from the initial state to a new one designated as (2). During this transition of states, energy will be exchanged with the elastic medium, as given by the first law of thermodynamics:

$$dU^t + \delta E^t = \delta Q^t + \delta C^t + \delta W^t, \tag{2.1}$$

where dU^t is the change in internal energy, δE^t the change in kinetic energy, δQ^t the change in heat energy, δC^t the change in chemical energy by atomic diffusion, and δW^t the change in its mechanical energy. The left-hand side of Eq. (2.1) represents the total change in the energy of the body. We will ignore here changes in kinetic energy, and restrict the applications of the present model to dislocation speeds less than approximately half of the transverse sound speed.[46–48]

Now the total internal energy can be written as a volume integral: $dU^t = \int_\Omega dU d\Omega$, where dU is the specific (per unit volume) change of the internal energy. The mechanical power (commonly known as the rate of Peach-Koehler work) is composed of two parts: (1) change in the elastic energy stored in the medium upon loop motion under the influence

of its own stress. This is precisely the change in the loop self-energy within a time interval δt, (2) the rate of work done on moving the loop as a result of the action of external and internal stresses, excluding the stress contribution of the loop itself. Thus $\delta W^t = \int_\Omega \sigma_{ik} d\epsilon_{ik} d\Omega$. The change in the total chemical energy can be written as a volume integral of the chemical potential μ_i, over the atomic concentration change dn_i. This is negative by convention for mass transport out of the volume. Additionally, if loop motion produces lattice defects (e.g., jogs and vacancies), chemical energy is deposited. Thus $\delta C^t = \int_\Omega (dP_d - \Sigma_i \mu_i dn_i) d\Omega$. Here, dP_d is the specific energy change associated with defect production. Finally, the net change in heat is composed of two parts: (1) heat energy (dH^*) generated by the loop as a result of atomic damping mechanisms (e.g., phonon and electron damping), and (2) heat transported across the boundary to the external reservoir, which is negative by convention. Hence, we have: $\delta Q^t = \int_\Omega dH^* d\Omega - \int_{\mathcal{S}} \mathbf{Q} \cdot d\mathbf{S}$. Here $\mathbf{Q}$ is the outgoing heat flux at the boundary. Using the divergence theorem for boundary integrals, we obtain

$$\int_\Omega \left[(dU - dH^* - dP_d) + \left(Q_{k,k} + \sum_i \mu_i dn_i - \sigma_{ik} d\epsilon_{ik} \right) \right] d\Omega = 0. \tag{2.2}$$

We will denote the enthalpy change $dH = dH^* + dP_d$, as the energy dissipated in defect generation and as heat. It is noted that in the special case where there is no heat or mass transport (i.e., $Q_{i,i} = dn_i = dP_d = 0$), no loop motion (i.e., $\delta W_{PK} = 0$), and under a hydrostatic stress field (i.e., $\sigma_{ik} = -P\delta_{ik}$), we get $\sigma_{ik} d\epsilon_{ik} = -P\delta_{ik} d\epsilon_{ik} = -P d\epsilon_{ii} = -P dV$, for a unit initial volume. Thus, we recover the familiar relationship between enthalpy and internal energy $dU = dH - PdV$. For an isothermal process, the Gibbs energy change is given by $dG = dH - TdS$. Thus,

$$\delta G^t = \int_\Omega \left[(dU - TdS) + \left(Q_{i,i} + \sum_i \mu_i dn_i - \sigma_{ik} d\epsilon_{ik} \right) \right] d\Omega. \tag{2.3}$$

The Clausius-Duhem statement of the second law of thermodynamics dictates that loop motion must increase the total entropy of the body and its surroundings.[49,50] Accordingly, we construct the following entropy production inequality for the solid:

$$\delta\Phi^t = \delta S^t - B - \int_{\mathcal{S}} \boldsymbol{\Xi} \cdot d\mathbf{S} \geqslant 0, \tag{2.4}$$

where $\delta\Phi^t \equiv \int_\Omega \Phi d\Omega$ is the total *entropy production* during δt, δS^t the total change in entropy, b the *local entropy source* per unit volume with $B \equiv \int_\Omega b d\Omega$, and $\boldsymbol{\Xi}$ the *entropy influx* due to heat input across the boundary $\mathcal{S}$. Utilizing the divergence theorem again in Eq. (2.4), we obtain the following inequality per unit volume:

$$\Phi = \delta S - b - \Xi_{k,k} \geqslant 0. \tag{2.5}$$

Now, the entropy flux crossing the boundary is $\boldsymbol{\Xi} = \mathbf{Q}/T$, and the flux divergence is given by

$$\Xi_{k,k} = \left(\frac{Q_k}{T} \right)_{,k} = \frac{1}{T} Q_k (\ln T)_{,k} - \frac{1}{T} Q_{k,k}, \tag{2.6}$$

while the local entropy source is given by

$$B = \int_\Omega \frac{dH}{T} = \int_\Omega \frac{1}{T} \left[dU + Q_{k,k} - \sigma_{ik} d\epsilon_{ik} + \sum_i \mu_i dn_i \right] d\Omega. \tag{2.7}$$

Substituting Eqs. (2.6) and (2.7) into Eq. (2.4), we obtain

$$\int_\Omega \left\{ (dU - TdS) + Q_k (\ln T)_{,k} - \sigma_{ik} d\epsilon_{ik} + \sum_i \mu_i dn_i \right\} d\Omega \leqslant 0. \tag{2.8}$$

Comparing the entropy production inequality (2.8) with Eq. (2.3), we can immediately see that a consequence of irreversibility (i.e., entropy production) is a *decrease* in Gibbs free energy. Following arguments similar to Erringen,[49] we write the internal energy in terms of entropy variation as

$$\delta G^t = \int_\Omega \left[\left(\frac{\partial U}{\partial S} - T \right) \delta S + Q_k (\ln T)_{,k} - \sigma_{ik} d\epsilon_{ik} + \sum_i \mu_i dn_i \right] d\Omega \leqslant 0. \tag{2.9}$$

Since the inequality must be valid for all variations of δS, its coefficient must vanish.[49,50] Thus,

$$\delta G^t = \int_\Omega \left[Q_k (\ln T)_{,k} - \sigma_{ik} d\epsilon_{ik} + \sum_i \mu_i dn_i \right] d\Omega \leqslant 0. \tag{2.10}$$

Under conditions where heat generation during dislocation motion is significant (e.g., high-speed deformation), additional equations must be solved for coupled point defect and heat conduction. Thus, equations for point-defect conservation, as well as generalized forms of Fick's and Fourier laws must be added. These are expressed in the following:

$$C^\gamma_{,t} = G^\gamma + J^\gamma_{k,k}, \tag{2.11}$$

$$J^\gamma_k = -D^\gamma_{ik} C_{,i} - D_{ik} \left(\frac{Q^* C}{kT^2} \right) T_{,i}, \tag{2.12}$$

$$Q_{\alpha,t} = Q''' - \kappa_{ik} T_{,i} - Q^* D_{i\alpha} C_{,i}, \tag{2.13}$$

where G^γ is the specific defect production rate, $\kappa_{i\alpha}$ is the thermal conductivity tensor, D^γ_{ik} the diffusion tensor of defect γ, Q^* the heat of transport, Q''' is the specific heat generation rate from plastic work, and $Q_{k,t}$ the rate of change of the thermal energy.

We treat here the special case where thermal effects are small [i.e., the first term in Eq. (2.10) is ignored]. We also consider climb motion to result from point defect absorption [i.e., the third term in Eq. (2.10) is summed over only vacancies and interstitials]. In Eq. (2.10), the volume integrals of the elastic term and the chemical term (osmotic) can be converted to line integrals over the dislocation loop. The stress tensor acting on any point is decomposed into a contribution resulting from the loop itself (i.e., self-stress $\sigma^{(s)}_{ik}$), and a

contribution resulting from other dislocations, defects, Peierls stress, and the applied stress field (i.e., external stress $\sigma_{ik}^{(e)}$). Thus, when the stress tensor in Eq. (2.10) is written as $\sigma_{ik}=\sigma_{ik}^{(s)}+\sigma_{ik}^{(e)}$, the elastic energy contributes two terms to Gibbs energy, while the chemical energy results in one additional term. We outline in the following how these three contributions can be converted to line integrals over the loop.

Now consider an infinitesimal variation in the position of a dislocation loop, depicted by the motion of the segments $\cup(AB,BC,CD,\ldots)$ in a time interval δt. During this motion, the dislocation line length has changed from L to $L+\Delta L$. The dislocation line vector is denoted by $\mathbf{s}=\mathbf{t}|\mathbf{s}|$, where $\mathbf{t}$ is a unit tangent vector. The change in position for atoms on the dislocation line is described by the vector $\delta\mathbf{r}$. For the change in the amount of work done on the dislocation loop during its transition from state (1) to state (2) in Fig. 1 above, we assume that the stress field is uniformly acting on every surface element $\mathbf{dA}=\mathbf{b}\times d\mathbf{s}$. The associated element of virtual force is: $d\mathbf{F}=\boldsymbol{\Sigma}\cdot\mathbf{dA}$. During loop motion from state (1) to state (2), the variation in this Peach-Koehler work[51] obtained by integration along the path Γ is given by

$$\begin{aligned}\int_\Omega [\sigma_{ik}d\epsilon_{ik}]^{(e)}d\Omega=\delta W_{PK}&=\oint_\Gamma d\mathbf{F}\cdot\delta\mathbf{r}\\&=\oint_\Gamma(\mathbf{b}\times d\mathbf{s}\cdot\boldsymbol{\Sigma})\cdot\delta\mathbf{r}\\&=\oint_\Gamma(\mathbf{b}\cdot\boldsymbol{\Sigma}\times\mathbf{t})\cdot\delta\mathbf{r}|d\mathbf{s}|\\&=\oint_\Gamma(\in_{ijk}\sigma_{jm}b_m t_k\delta r_i)|d\mathbf{s}|.\end{aligned}\tag{2.14}$$

Ghoniem and Sun[52–54] showed that the stress tensor of a loop ensemble can be written as a fast numerical sum, given by

$$\sigma_{ij}=\frac{\mu}{4\pi}\sum_{\gamma=1}^{N_{loop}}\sum_{\beta=1}^{N_s}\sum_{\alpha=1}^{Q_{max}}b_n w_\alpha\left[\frac{1}{2}R_{,mpp}(\in_{jmn}r_{i,u}+\in_{imn}r_{j,u})+\frac{1}{1-\nu}\in_{kmn}(R_{,ijm}-\delta_{ij}R_{,ppm})r_{k,u}\right].\tag{2.15}$$

In Eq. (2.15) above, the fast sum is carried over the number of loops (N_{loop}), the number of parametric segments within each loop (N_s), and the number of quadrature points on each curved segment (Q_{max}). The third-order tensor $R_{,\alpha\beta\gamma}$ contains successive derivatives of the radius vector $\mathbf{R}$ connecting a point on the dislocation loop to a field point, $r_{k,u}$ are parametric derivatives of the Cartesian components, which describe the 3D dislocation segment as a function of the parameter (u).[52–54] The shear modulus is μ, w_α are weight functions at the quadrature point set $\{\alpha\}$ on the curved segment, and $\in_{ijk}$ is the permutation tensor.

The total self-energy of the dislocation loop is obtained by double integrals along the contour Γ. Gavazza and Barnett[55] have shown that the first variation in the self-energy of the loop can be written as a single line integral of the form:

$$\begin{aligned}\int_\Omega[\sigma_{ik}d\epsilon_{ik}]^{(s)}d\Omega&=\oint_\Gamma\left(\left[E(\mathbf{t})-[E(\mathbf{t})+E''(\mathbf{t})]\ln\left(\frac{8}{\varepsilon\kappa}\right)\right]\kappa-J(L,\mathbf{P})\right)\mathbf{n}\cdot\delta\mathbf{r}|d\mathbf{s}|+[\delta U]_{core},\end{aligned}\tag{2.16}$$

where $\mathbf{n}$ is normal to the dislocation line vector $\mathbf{t}$ on the glide plane, and $\varepsilon=|\mathbf{b}/2|$ is the dislocation core radius.[56] The first term results from loop stretching during the infinitesimal motion, the second and third are the *line tension* contributions, while $J(L,\mathbf{P})$ is a nonlocal contribution to the self-energy. The dominant contributions to the self-energy (or force) are dictated by the local curvature κ, and contain the prelogarithmic energy term $E(\mathbf{t})$ for a straight dislocation tangent to the loop at point $\mathbf{P}$, and its second angular derivative E''. $[\delta U]_{core}$ is the contribution of the dislocation core to the self-energy. Defining the angle between the Burgers vector and the tangent as $\alpha=\cos^{-1}(\mathbf{t}\cdot\mathbf{b}/|b|)$, Gore[57] showed that a convenient form of the self-energy integral for an isotropic elastic medium of $\nu=\frac{1}{3}$ can be written as

$$\begin{aligned}\int_\Omega[\sigma_{ik}d\epsilon_{ik}]^{(s)}d\Omega=\oint_\Gamma\Bigg\{&-\kappa[E(\alpha)+E''(\alpha)]\ln\left(\frac{8}{\varepsilon\kappa}\right)\\&+\mu b^2\Bigg[\kappa\left(\frac{21+\cos^2\alpha}{64\pi}\right)\\&+\bar{\kappa}\left(\frac{2\cos^2\alpha-1}{2\pi}\right)\Bigg]\Bigg\}\mathbf{n}\cdot\delta\mathbf{r}|d\mathbf{s}|,\end{aligned}\tag{2.17}$$

where the energy prefactors are given by $E(\alpha)=[\mu b^2/4\pi(1-\nu)](1-\nu\cos^2\alpha)$, and $E''(\alpha)$ is its second angular derivative. Accurate numerical calculations of the self-energy of any complex-shape loop have been performed by Ghoniem and Sun,[54] where the double line integral is converted to a fast summation over the loop segments and quadrature points. However, a purely numerical method for evaluation of the self-energy requires intensive computations because of the need to use large quadrature order for good accuracy.[54] Equation (2.17) is an alternate convenient approximation, in which the contributions of various terms are easily computed. Schwarz[41] conducted a numerical study to determine the effects of various terms on the self-force, and concluded that the major contribution results from the first two terms in Eq. (2.17), which are the usual line tension approximation. However, the relative importance of the third term (which represents contributions from the dislocation core and dislocation line stretching) and fourth term (which is an approximation to nonlocal contributions from other parts of the loop) can be seen by a simple argument. The nonlocal term is obtained by approximating the loop as a pure shear loop at an average curvature of $\bar{\kappa}$. For a reasonable size loop of approximate radius in the range $1000-10\,000|\mathbf{b}|$, it can be shown that the total contribution of nonlocal, core and stretch terms is on the order of less than 18%. The contribution of the nonlocal term is about half of this amount for purely edge components. Hence, a computa-

tionally efficient and very accurate method is obtained when all contributions are combined in Eq. (2.17).

Absorption of point defects by dislocation segments can be treated by considering the influence of the chemical term in Eq. (2.10) on its motion. Incorporation of atomic defects into dislocation cores leads to dislocation climb. The thermodynamic force associated with this motion is referred to as the *osmotic* force. During climb motion of atoms within the dislocation core, the number of vacancies (or interstitials) per unit length dn_γ/L, changes by the amount

$$\frac{dn_\gamma}{L}=\frac{|\mathbf{b}|\mathbf{m}\cdot\delta\mathbf{r}}{\Omega_\gamma}, \tag{2.18}$$

where Ω_γ is the vacancy (interstitial) volume, and $\mathbf{m}$ is a unit vector normal to the glide plane. The change in chemical potential per vacancy (interstitial) is given by

$$\mu_\gamma=kT\ln\left(\frac{C_\gamma}{C_\gamma^{eq}}\right). \tag{2.19}$$

Here C_γ is the nonequilibrium concentration of vacancies (or interstitials). C_γ may result from quenching, sudden temperature variation, irradiation, externally applied stress,[58] or dislocation segment annihilation and intersection. C_γ^{eq} is the thermodynamic equilibrium concentration of the atomic defect. The corresponding contribution from point defect flow to the variation in Gibbs energy for the entire loop can now be obtained by line integration. Incorporating Eqs. (2.14), (2.17), (2.18), and (2.19) into inequality (2.10), we obtain

$$\delta G^t=-\oint_\Gamma(\mathbf{f}_S+\mathbf{f}_O+\mathbf{f}_{PK})\cdot\delta\mathbf{r}|d\mathbf{s}|\leqslant 0, \tag{2.20}$$

where we define the following generalized thermodynamic forces: $\mathbf{f}_{PK}\equiv$ the *Peach-Koehler force* per unit length $=\mathbf{b}\cdot\boldsymbol{\Sigma}\times\mathbf{t}$, $\mathbf{f}_S\equiv$ the *self-force* per unit length

$$\left\{-\kappa[E(\alpha)+E''(\alpha)]\ln\left(\frac{8}{\varepsilon\kappa}\right)+\mu b^2\left[\kappa\left(\frac{21+\cos^2\alpha}{64\pi}\right)+\kappa\left(\frac{2\cos^2\alpha-1}{2\pi}\right)\right]\right\}\mathbf{n},$$

$\mathbf{f}_O\equiv$ the total *osmotic force*[46] for defect γ per unit length, $=-\Sigma_\gamma\gamma kT(|\mathbf{b}|/\Omega_\gamma)\ln(C_\gamma/C_\gamma^{eq})\,\mathbf{m}$ where $\gamma=(-1)$ for vacancies and $(+1)$ for interstitials.

In compact tensor form, Eq. (2.20) can be written as

$$\delta G^t=-\oint_\Gamma f_k^t\delta r_k|d\mathbf{s}|\leqslant 0, \tag{2.21}$$

where f_k^t is the k component of the total force: $\mathbf{f}^t=\mathbf{f}_S+\mathbf{f}_O+\mathbf{f}_{PK}$, and δr_k is the displacement of core atoms in the k direction.

III. VARIATIONAL FORMULATION

A. Governing integral equation of motion

Inequality (2.10) suggests that the components of Gibbs energy can be written as *conjugate* pairs, representing the inner products of *generalized thermodynamic forces* and *generalized displacements*. The equations of motion can thus be obtained if one defines an appropriate set of generalized coordinates and conjugate generalized thermodynamic forces, in such a way as to result in entropy production and a corresponding decrease in δG during a virtual infinitesimal transition. Let us assume that atoms within the dislocation core are transported in some general drift force field, as a consequence of the motion of atomic size defects (e.g., vacancies, interstitials, kinks, and jogs). The drift velocity of each atom is given by Einstein's mobility relationship: $\mathbf{V}_\lambda=(1/kT)\mathbf{D}\mathbf{f}_\lambda$, where $\mathbf{V}_\lambda$ is the drift velocity, $\mathbf{D}$ is a diffusion tensor, and $\mathbf{f}_\lambda$ is a generalized thermodynamic force representing process λ. Similarly, the flux resulting from a given process can be related to a corresponding thermodynamic force. We consider here three thermodynamic forces: (1) forces of mechanical origin (i.e., *Peach-Koehler forces*), as a result of variations in virtual work on the dislocation loop and variations in the stored elastic energy in the medium when the dislocation changes its shape, (2) gradients in point defect concentrations within the surrounding medium (i.e., *chemical forces*), and finally (3) temperature gradient forces associated with heat flow.

A generalization of the previous analysis can be accomplished if one postulates that near equilibrium, thermodynamic forces are sufficiently *weak* that we might expand the flux in a power series in $\mathbf{f}_\lambda$.[59] Let us denote $\mathbf{J}_k\{\mathbf{f}_\lambda\}$ as type-k flux as a result of a generalized thermodynamic force λ, $\{\mathbf{f}_\lambda\}$. Thus, a generalization of Einstein's phenomenological transport relationship is given by

$$\mathbf{J}_k\{\mathbf{f}_\lambda\}=\mathbf{J}_k(0)+\sum_\lambda\left(\frac{\partial\mathbf{J}_k}{\partial\mathbf{f}_\lambda}\right)_0\mathbf{f}_\lambda+\frac{1}{2}\sum_{\lambda m}\left(\frac{\partial^2\mathbf{J}_k}{\partial\mathbf{f}_\lambda\partial\mathbf{f}_m}\right)_0\mathbf{f}_\lambda\mathbf{f}_m+\cdots. \tag{3.1}$$

In the linear range of irreversible processes, Eq. (3.1) is restricted to only the first two terms in the expansion. Moreover, at thermodynamic equilibrium in the absence of generalized forces, all modes of atom transport vanish, and the first term, $\mathbf{J}(0)$, is identically zero. Taking the velocity of atoms on the dislocation line (i.e., representing the core) to be proportional to the atomic flux, and defining generalized mobilities via the tensor $\mathbf{L}$ with components: $L_{ij}=(\partial\mathbf{V}_i/\partial\mathbf{f}_j)_0$, the phenomenological relationship [Eq. (3.1)] is simplified to

$$\mathbf{V}_\beta\{\mathbf{f}_\lambda\}=\sum_\lambda L_{\beta\lambda}\mathbf{f}_\lambda. \tag{3.2}$$

Measurements of dislocation speed[47] reveal that the velocity is a nonlinear function of the local shear stress, and that it is limited by the Rayleigh wave speed. At dislocation speeds close to this limit, one must account for inertial effects.[48] In practice, however, most DD simulations have assumed a nonlinear stress-velocity relationship, with exponents that are adjusted over specified stress ranges.[19,20] Over a small range of local forces, a linearization technique can be invoked to allow for incremental utilization of the relationship given by Eq. (3.2).

As a consequence of the increase in entropy production Φ, or equivalently the decrease in Gibbs energy δG,

Prigogine[59] showed that $L_{\beta\lambda}\mathbf{f}_\beta\mathbf{f}_\lambda \geq 0$. This relationship gives a positive definite quadratic form, which imposes restrictions on the matrix of coefficients to be positive. The generalized *mobilities* L_{ij} are subject to additional temporal symmetries as a result of the principle of detailed balance, as shown by Onsager:[60] $L_{\beta\lambda}=L_{\lambda\beta}$. The mobility matrix relates the influence of an independent thermodynamic force of the λ type to the partial flux of the *k* type. In most applications of DD so far, the mobility matrix $L_{\lambda\beta}$ is assumed to be diagonal and independent of the type of thermodynamic force. However, we will assume that dislocation mobility is spatially anisotropic, since the speed of screw segments is usually smaller than edge segments as a consequence of the crystal structure. These simplifications lead to direct proportionality between the velocity and total force along each independent direction. Thus, we can denote $B_{\alpha k}$ as a diagonal resistivity (inverse mobility) matrix, and substitute in Eq. (2.21) to obtain the following equivalent form of the Gibbs energy variation:

$$\delta G^t = -\oint_\Gamma B_{\alpha k} V_\alpha \delta r_k |d\mathbf{s}| \leq 0. \tag{3.3}$$

The resistivity matrix can have three independent components (two for glide and one for climb), depending on the crystal structure and temperature. It is expressed as

$$[B_{\alpha k}] = \begin{bmatrix} B_1 & 0 & 0 \\ 0 & B_2 & 0 \\ 0 & 0 & B_3 \end{bmatrix}. \tag{3.4}$$

Combining Eq. (2.21) with Eq. (3.3), we have

$$\oint_\Gamma (f_k^t - B_{\alpha k} V_\alpha)\, \delta r_k |d\mathbf{s}| = 0. \tag{3.5}$$

The magnitude of the virtual displacement δr_k is not specified, and hence can be arbitrary. This implies that Eq. (3.5) represents force balance on every atom of the dislocation core, where the acting force component f_k^t is balanced by viscous dissipation in the crystal via the term $B_{\alpha k}V_k$. However, this is not necessarily desirable, because one needs to reduce the independent degrees of freedom that describe loop motion, yet still satisfies the laws of irreversible thermodynamics described here. To meet this end, we develop a general method, with greatly reduced degrees of freedom for the motion of dislocation core atoms.

B. The Galerkin method

Assume that the dislocation loop is divided into N_s curved segments. The line integral in Eq. (3.5) can be written as a sum over each parametric segment *j*, i.e.,

$$\sum_{j=1}^{N_s} \int_j \delta r_i (f_i^t - B_{ik} V_k) |d\mathbf{s}| = 0. \tag{3.6}$$

Note that in Eq. (3.6), we sum over the number of segments *j* and follow the standard rules of 3D tensor analysis. We now choose a set of generalized coordinates q_m at the two ends of each segment *j*. Then, the segment can be parametrically described as

$$r_i = \sum_{m=1}^{N_{DF}} \mathcal{C}_{im}(u) q_m, \tag{3.7}$$

where $\mathcal{C}_{im}(u)$ are shape functions, dependent on the parameter u $(0 \leq u \leq 1)$. Equation (3.7) is a general parametric representation of the dislocation line for segment *j*. Possible convenient parameterization methods are discussed in Refs. [52–54]. In Sec. IV we introduce quintic splines as flexible and convenient parametric curves for complex dislocation loop geometry, while the applications in Sec. V illustrate the utilization of several types of parametric elements on the same loop. It is noted that the index *m* is assumed to be summed from 1 to N_{DF}, where N_{DF} is the number of total generalized coordinates at two ends of the loop segment. Accordingly, the three components of the displacement vector are given by

$$\delta r_i = \sum_{m=1}^{N_{DF}} \mathcal{C}_{im}(u)\, \delta q_m. \tag{3.8}$$

On the other hand, we have for the velocity of any point on the dislocation line, within segment *j*:

$$V_k = r_{k,t} = \sum_{n=1}^{N_{DF}} \mathcal{C}_{kn} q_{n,t}. \tag{3.9}$$

And the arc length differential for segment *j* is given by

$$|d\mathbf{s}| = (r_{l,u} r_{l,u})^{1/2} du = \left(\sum_{p,s=1}^{N_{DF}} q_p \mathcal{C}_{lp,u} \mathcal{C}_{ls,u} q_s \right)^{1/2} du. \tag{3.10}$$

An ensemble of dislocation loops is considered a continuous dynamical system, where every point on dislocation lines is subject to continuous displacement. The finite element process in continuum mechanics is based on approximating the continuous displacement field by a linear combination of piece-wise known shape functions over specified domains. To obtain the unknown coefficients in the linear combination, an integral form of the governing equation is formulated, and an element-by-element assembly is extracted. The result is a system of equations for *standard discrete systems*, which can be handled by numerical methods. We will follow a similar approach here, in which the weight functions in the integral form are the same as the shape functions of the problem. Minimization of the weighted residuals results in symmetric matrices, which simplifies integration of the equations of motion. This variational approach is thus coincident with the Galerkin method as a special case of the method of weighted residuals. Recently, a number of investigators formulated microstructure evolution problems in a similar manner.[61,62]

At this point, we may substitute Eqs. (3.8), (3.9), and (3.10) into the governing Eq. (3.6), and obtain the following form:

$$\sum_{j=1}^{N_s}\int_0^1\sum_{m=1}^{N_{DF}}\delta q_m\mathcal{C}_{im}(u)\left[f_i^t-B_{ik}\sum_{n=1}^{N_{DF}}\mathcal{C}_{kn}q_{n,t}\right]\times\left(\sum_{p,s=1}^{N_{DF}}q_p\mathcal{C}_{lp,u}\mathcal{C}_{ls,u}q_s\right)^{1/2}du=0. \tag{3.11}$$

Appropriate collection of terms into more convenient functions can reduce the apparent complexity of this form of the equation of motion. We will define here two such functions: an effective force and an effective resistivity. A *generalized force*, f_m, is defined as

$$f_m=\int_0^1 f_i^t\mathcal{C}_{im}(u)\left(\sum_{p,s=1}^{N_{DF}}q_pN_{lp,u}N_{ls,u}q_s\right)^{1/2}du, \tag{3.12}$$

while a *resistivity matrix* element, γ_{mn}, is given by

$$\gamma_{mn}=\int_0^1\mathcal{C}_{im}(u)B_{ik}\mathcal{C}_{kn}(u)\left(\sum_{p,s=1}^{N_{DF}}q_p\mathcal{C}_{lp,u}\mathcal{C}_{ls,u}q_s\right)^{1/2}du. \tag{3.13}$$

It is noted that $[\gamma_{mn}]$ is a symmetric matrix because of the structure of the above definition and symmetric mobilities. With these two parameters defined above, the variational integral form of the Gibbs energy equation is readily transformed to a discrete form, given by

$$\sum_{j=1}^{N_s}\left[\sum_{m=1}^{N_{DF}}\delta q_m\left(f_m-\sum_{n=1}^{N_{DF}}\gamma_{mn}q_{n,t}\right)\right]=0. \tag{3.14}$$

For the entire dislocation loop, we map all local degrees of freedom $q_i^{(j)}$ of each segment j onto a set of global coordinates, such that the global coordinates are equal to the local coordinates at each beginning node on the segment:

$$\{q_1^{(1)},q_2^{(1)},q_3^{(1)},\ldots,q_1^{(2)},q_2^{(2)},q_3^{(2)},\ldots\}=\{Q_1,Q_2,Q_3,\ldots,Q_N\}^T, \tag{3.15}$$

where N is the total number of degrees of freedom of the loop. Similar to the finite element procedure, the local segment resistivity matrix $[\gamma_{mn}]$ is added into corresponding global locations in the global resistivity matrix $[\Gamma_{kl}]$, such that

$$\sum_{j=1}^{N_s}\sum_{m=1}^{N_{DF}}\sum_{n=1}^{N_{DF}}[\delta q_m\gamma_{mn}q_{n,t}]^{(j)}=\sum_{k=1}^{N_{tot}}\sum_{l=1}^{N_{tot}}\delta Q_k\Gamma_{kl}Q_{l,t}, \tag{3.16}$$

where $N_{tot}=N_sN_{DF}$ is the total number of degrees of freedom for the loop. The global resistivity matrix $[\Gamma_{kl}]$ is also symmetric and banded or sparse. The component Γ_{kl} is zero if the degrees of freedom k and l are not connected through a segment. In addition, the global force vector $\{\mathcal{F}_k\}$ can similarly be represented as

$$\sum_{j=1}^{N_s}\sum_{m=1}^{N_{DF}}[\delta q_mf_m]^{(j)}=\sum_{k=1}^{N_{tot}}\delta Q_k\mathcal{F}_k. \tag{3.17}$$

Therefore, Eq. (3.14) can be expressed as

$$\sum_{k=1}^{N_{tot}}\delta Q_k\left(\mathcal{F}_k-\sum_{l=1}^{N_{tot}}\Gamma_{kl}Q_{l,t}\right)=0. \tag{3.18}$$

Since the virtual displacements in the generalized coordinates are totally arbitrary, the previous equation can only be satisfied if

$$\mathcal{F}_k=\sum_{l=1}^{N_{tot}}\Gamma_{kl}Q_{l,t}. \tag{3.19}$$

Equation (3.19) represents a set of time-dependent ordinary differential equations, which describe the motion of dislocation loops as an evolutionary dynamical system. Similar microstructure evolution equations have been derived by Suo[62] in connection with grain and void growth phenomena. Furthermore, the above spatially resolved equations can be discretized in time by the so-called *generalized trapezoidal family of methods*[63] as

$$\sum_{l=1}^{N_{tot}}\Gamma_{kl}^{(n+\alpha)}Q_l^{(n+1)}=\sum_{l=1}^{N_{tot}}\Gamma_{kl}^{(n+\alpha)}Q_l^{(n)}+\Delta t\mathcal{F}_k^{(n+\alpha)}, \tag{3.20}$$

where Δt is the time-step and n is the time-step index. In addition, α is a parameter, which determines explicit or implicit time-integration, taken to be in the interval [0,1] such that: $\alpha=0$ for forward difference integration (Euler), $\alpha=1/2$ for midpoint or trapezoidal integration, $\alpha=2/3$ for Galerkin integration, and $\alpha=1$ for backward difference (Euler) integration.[63]

IV. COMPUTATIONAL GEOMETRY OF DISLOCATION LOOPS

A. Curved spline parametrization

Recently, simplified parametric representation of 2D dislocation loops has been successfully implemented.[64] In the following, however, we develop a more general method for geometric representation of 3D dislocation loops. Each dislocation loop is described as a composite spline curve, made up by connecting curved segments together at their common nodes. Each segment is described as an independent parametric space curve, with the parameter u varying in the range 0 to 1. A general vector form of the dislocation line equation for segment (j) can be expressed as

$$\mathbf{r}^{(j)}(u)=\sum_{i=0}^{n}\mathbf{A}_i^{(j)}u^i, \tag{4.1}$$

where n is a polynomial order and $\mathbf{A}_i$ represent the associated vector coefficients. The value of n determines the segment type. Thus, when $n=1$ the segment is a straight line, when $n=3$ the segment is a cubic polynomial, and when $n=5$, the segment is a fifth-order (quintic) polynomial. The coefficients $\mathbf{A}_i$ are determined by boundary conditions imposed on beginning and end nodes. These boundary conditions can be described in terms of specified geometric properties, such as the nodal position, tangent, curvature, and torsion.

In the following, we restrict ourselves to the more general quintic spline representation of loops. Composite linear and

cubic spline shapes can be easily determined by a similar approach. The six coefficients of a quintic spline segment are determined by assigning six independent vectors, obtained from six boundary conditions. These are $\mathbf{r}^{(j)}(0)$, $\mathbf{r}^{(j)}(1)$, $\mathbf{r}^{(j)}_{,u}(0)$, $\mathbf{r}^{(j)}_{,u}(1)$, $\mathbf{r}^{(j)}_{,uu}(0)$, and $\mathbf{r}^{(j)}_{,uu}(1)$, where $\mathbf{r}^{(j)}_{,u}=d\mathbf{r}^{(j)}/du$ and $\mathbf{r}^{(j)}_{,uu}=d^2\mathbf{r}^{(j)}/du^2$. Geometrically, $\mathbf{r}^{(j)}(0)$ and $\mathbf{r}^{(j)}(1)$ are the position vectors of nodes j and $j+1$, i.e., $\mathbf{P}^{(j)}$ and $\mathbf{P}^{(j+1)}$. The vectors $\mathbf{r}^{(j)}_{,u}(0)$ and $\mathbf{r}^{(j)}_{,u}(1)$ are the tangent vectors of nodes j and $j+1$, i.e., $T^{(j)}_E\mathbf{t}^{(j)}$ and $T^{(j+1)}_B\mathbf{t}^{(j+1)}$, respectively, where $T^{(j)}_E$ and $T^{(j+1)}_B$ are magnitudes of tangent vectors at the end (E) and beginning (B) of each segment, while the unit vectors $\mathbf{t}^{(j)}$ and $\mathbf{t}^{(j+1)}$ are the dislocation sense vectors at nodes j and $j+1$, respectively. The vectors $\mathbf{r}^{(j)}_{,uu}(0)$ and $\mathbf{r}^{(j)}_{,uu}(1)$ are linear combinations of the tangent and normal vectors because they lie on the plane spanned by them. Because the resultant loop profile is a composite curve, dislocation line continuity may not be maintained at each node if boundary conditions on segments are arbitrarily assigned. In general, C^0(position) and C^1(tangent) continuity can be easily satisfied if we assign the same position and tangent vectors at each node. However, since self-forces on dislocation segments are proportional to the local curvature Eq. (2.17), C^2 continuity will ensure the continuity of self-forces at segment nodes as well. The curvature of a general point on segment j can be expressed as

$$\kappa^{(j)}(u)=\frac{\|\mathbf{r}^{(j)}_{,u}(u)\times\mathbf{r}^{(j)}_{,uu}(u)\|}{\|\mathbf{r}^{(j)}_{,u}(u)\|^3}. \tag{4.2}$$

To maintain C^2 continuity at each node, we let the curvature of the end point of segment j be equal to the curvature at the beginning node of curved segment $j+1$: $\kappa^{(j)}(1)=\kappa^{(j+1)}(0)$. Because $\mathbf{r}^{(j)}_{,uu}$ is a linear combination of $\mathbf{T}$ and $\mathbf{N}$, the tangent component of vector $\mathbf{r}^{(j)}_{,uu}$ does not influence the line curvature. Therefore, we can just assign the normal vectors $N^{(j)}_E\mathbf{n}^{(j)}$ and $N^{(j+1)}_B\mathbf{n}^{(j+1)}$ for $\mathbf{r}^{(j)}_{,uu}(1)$ and $\mathbf{r}^{(j+1)}_{,uu}(0)$, respectively, where N^j_E and $N^{(j+1)}_B$ represent magnitudes associated with the unit vectors $\mathbf{n}^{(j)}$ and $\mathbf{n}^{(j+1)}$. After substituting all boundary conditions into Eq. (4.1) and rearranging terms, we obtain

$$\mathbf{r}^{(j)}(u)=\mathcal{C}_1\mathbf{P}^{(j)}+\mathcal{C}_2\mathbf{P}^{(j+1)}+\mathcal{C}_3T^{(j)}_E\mathbf{t}^{(j)}+\mathcal{C}_4T^{(j+1)}_B\mathbf{t}^{(j+1)}+\mathcal{C}_5N^{(j)}_E\mathbf{n}^{(j)}+\mathcal{C}_6N^{(j+1)}_B\mathbf{n}^{(j+1)}. \tag{4.3}$$

Note that the superscript on the LHS of Eq. (4.3) refers to segment j, while on the RHS, it is associated with nodes j and $j+1$ on the same segment. The coefficients $\mathcal{C}_1$ to $\mathcal{C}_6$ are invariant shape functions, and can be expressed in terms of parameter $(0\leqslant u\leqslant 1)$ as

$$\mathcal{C}_1=-6u^5+15u^4-10u^3+1,$$

$$\mathcal{C}_2=6u^5-15u^4+10u^3,$$

$$\mathcal{C}_3=-3u^5+8u^4-6u^3+u,$$

$$\mathcal{C}_4=-3u^5+7u^4-4u^3,$$

$$\mathcal{C}_5=-0.5u^5+1.5u^4-1.5u^3+0.5u^2,$$

$$\mathcal{C}_6=0.5u^5-u^4+0.5u^3.$$

We can cast the parametric Eq. (4.3) into a convenient matrix form for a single parametric quintic spline of a segment, if we reorganize the generalized coordinates q_m as

$$\{q_m\}=\{q_1,q_2,q_3,\ldots,q_{18}\}^T, \tag{4.4}$$

where the first nine components are for the beginning node of the segment; with q_1-q_3 being three components of position, q_4-q_6 three components of the tangent vector, and q_7-q_9 three components of the normal vector. Correspondingly, q_{10} to q_{18} indicate all coordinates at the end of a segment. The shape functions for the quintic spline can also be organized in the following matrix form:

$$[\mathcal{C}_{im}]=\begin{bmatrix}\mathcal{C}_1&0&0&\mathcal{C}_3&0&0&\mathcal{C}_5&0&0&\mathcal{C}_2&0&0&\mathcal{C}_4&0&0&\mathcal{C}_6&0&0\\0&\mathcal{C}_1&0&0&\mathcal{C}_3&0&0&\mathcal{C}_5&0&0&\mathcal{C}_2&0&0&\mathcal{C}_4&0&0&\mathcal{C}_6&0\\0&0&\mathcal{C}_1&0&0&\mathcal{C}_3&0&0&\mathcal{C}_5&0&0&\mathcal{C}_2&0&0&\mathcal{C}_4&0&0&\mathcal{C}_6\end{bmatrix}. \tag{4.5}$$

With this notation, Eq. (4.3) can be cast in the computational form of Eq. (3.7). The total number of available degrees of freedom for a *free* quintic spline segment is thus equal to the number of components in the Cartesian vector q_m, i.e., $N_{DF}=6\times3=18$. However, because of geometric and physical restrictions on dislocation motion, N_{DF} can be greatly reduced, as we will discuss next.

B. Constrained glide motion and reduced degrees of freedom

It is apparent that general dislocation motion would involve many degrees of freedom N_{DF} in the most general case. Fortunately, however, N_{DF} is small in practice. As a result of segment connectivity at common nodes, only half of the total DF's are required per segment, and $N_{DF}=9$ for general 3D motion, and $N_{DF}=6$ for motion on a glide plane. The direction of the Peach-Koehler force imposes additional constraints. As can be seen from Eqs. (2.14) and (2.17), both external and self-forces on a dislocation node are along the normal direction $\mathbf{n}$ on the glide plane. Also, because $\mathbf{n}\cdot\mathbf{t}=0$, N_{DF} is reduced further from 6 to 4 for 2D glide motion; that is one for the displacement magnitude, two for the tangent vector, and one for the magnitude of the normal. Furthermore, we introduce here two additional conditions, which simplify the loop profile calculations even further. A *smoothness* condition is invoked such that rapid variations of curvature are avoided when two segments of vastly different lengths are connected via a composite spline. If the magni-

tude of the tangent is not related to nodal positions, undesirable *cusps* may develop on the dislocation line. Thus, we take the magnitude of the tangent vector to be estimated from the arc length between previous nodal positions on the segment. This criterion is exact when the parameter $u=s$, where s is the arc length itself. On the other hand, the line curvature can be independently computed from the dislocation configuration and nodal loading in a simple manner. If the forces at the node are not near equilibrium (i.e., the acting forces are much larger than the self-force), the curvature is determined from three neighboring nodes on the dislocation line. On the other hand, near equilibrium (e.g., close to strong pinning points), the curvature of a node is readily computed from Eq. (2.17), once the local external force is known. These approximations can lead to an additional reduction of two degrees of freedom, and we are left with solving for only two equations per node. These constraints can be relaxed, if one is interested in more complex details of dislocation motion. We will show later in Sec. V that dislocation glide motion can be adequately described in most cases with only two degrees of freedom per node.

We derive here constrained discrete equations of motion, when dislocation lines are confined to their glide plane. In this special case, there is a total of six independent unknowns. That is, $\Delta P_x, \Delta P_y, \Delta T_x, \Delta T_y, \Delta N_x, \Delta N_y$, which correspond to incremental displacements, tangents, and normals in the x and y directions, respectively. Let us first consider the geometric constraints. Because the normal is always perpendicular to the tangent at the node, we have: $(\mathbf{T}^{(i)}+\Delta\mathbf{T})\cdot(\mathbf{N}^{(i)}+\Delta\mathbf{N})=0$, where the symbols with superscript (i) refer to a previous time-step of known values (i.e., $\mathbf{T}^{(i+1)}=\mathbf{T}^{(i)}+\Delta\mathbf{T}$). Furthermore, from a geometric point of view, the curvature of the loop at a current time-step is related to the normal and tangent vectors as $\kappa=||\mathbf{N}||/||\mathbf{T}||^2$. Where the curvature is assumed to be determined by local forces or nodal positions, as discussed earlier. The norm (magnitude) of the current tangent vector is proportional to the previous arc length of a segment. That is $||\mathbf{T}||=\eta$, where η is determined by the arc length of the previous time-step. Finally, the displacement vector is perpendicular to the tangent direction of the considered node,

$$\frac{\Delta P_y}{\Delta P_x}=-\frac{T_x^{(i)}}{T_y^{(i)}}=\gamma, \tag{4.6}$$

where γ is a constant determined by previous tangent components. Thus, by introducing an angle θ, which is the angle between the tangent vector and the x direction, the six independent unknowns can be reduced to only two: ΔP_x and θ, such that all constraints are automatically satisfied:

$$\Delta P_x=\Delta P_x, \quad \Delta P_y=\gamma\Delta P_x, \tag{4.7}$$

$$\Delta T_x=\eta\cos\theta-T_x^{(i)}, \quad \Delta T_y=\eta\sin\theta-T_y^{(i)}, \tag{4.8}$$

$$\Delta N_x=-\kappa\eta^2\sin\theta-N_x^{(i)}, \quad \Delta N_y=\kappa\eta^2\cos\theta-N_y^{(i)}. \tag{4.9}$$

Moreover, a linearization technique can be used to approximate sine and cosine functions in terms of $\Delta\theta$, as long as the time step is small, and hence the tangent angle variation is small between time steps. Based on the above constraints, Eq. (3.8) may finally be simplified with a reduced set of shape functions $\tilde{\mathcal{C}}$ as

$$\{\delta x_i\}=[\tilde{\mathcal{C}}_{im}(u)]\{\delta q_m\}, \tag{4.10}$$

where

$$\{\delta r_i\}=\begin{Bmatrix}\delta x\\ \delta y\end{Bmatrix}, \quad \{\delta q_m\}=\begin{Bmatrix}\delta P_{xB}\\ \delta\theta_B\\ \delta P_{yE}\\ \delta\theta_E\end{Bmatrix},$$

$$[\tilde{\mathcal{C}}_{im}(u)]=\begin{bmatrix}\mathcal{C}_1 & \mathcal{D}_1 & \mathcal{C}_2 & \mathcal{D}_2\\ \gamma\mathcal{C}_1 & \mathcal{D}_3 & \gamma\mathcal{C}_2 & \mathcal{D}_4\end{bmatrix},$$

and

$$\mathcal{D}_1=-\eta_L\mathcal{C}_3\sin\theta_B-\kappa_B\eta_B^2\mathcal{C}_5\cos\theta_B, \tag{4.11}$$

$$\mathcal{D}_2=-\eta_E\mathcal{C}_4\sin\theta_E-\kappa_E\eta_E^2\mathcal{C}_6\cos\theta_E, \tag{4.12}$$

$$\mathcal{D}_3=\eta_L\mathcal{C}_3\cos\theta_B-\kappa_B\eta_B^2\mathcal{C}_5\sin\theta_B, \tag{4.13}$$

$$\mathcal{D}_4=\eta_E\mathcal{C}_4\cos\theta_E-\kappa_E\eta_E^2\mathcal{C}_6\sin\theta_E. \tag{4.14}$$

It is noted that the subscripts B and E refer to *beginning* and *end* nodes of one segment of the dislocation loop.

C. Adaptive protocols for node and time-step assignments

Because of the evolving nature of dislocation line geometry as a result of strong interactions, it is highly desirable to develop adaptive methods that capture essential physics without excessive computations. Control of the magnitude of the computational time-step and nodal positions on each segment has a direct influence on the final accuracy of DD simulations. For node redistribution, we first compute a reference curvature $\overline{\kappa}$ for the entire loop, which is normally taken as the average curvature of all nodes. Then, we compare the curvature κ_i of each node with $\overline{\kappa}$, and classify nodes into high curvature groups ($\kappa_i>\overline{\kappa}$) and low curvature groups ($\kappa_i<\overline{\kappa}$). Finally, we increase the number of nodes for each high curvature group and decrease the number of nodes for each low curvature group. After adding or removing nodes, we redistribute the nodes evenly for that group. To prevent the number of nodes from increasing or decreasing too fast, we only add or remove one node at a time. If the number of nodes for a low curvature group is less than a specified minimum, we keep the current nodes because a prescribed minimum number of nodes is required to maintain the loop geometry. After redistributing nodes on each segment, we calculate the displacement and tangent angle of each new node based on the current loop geometry. The radius of curvature of each new node is determined by a linear interpolation from old nodes for open loops, or by circular arc approximations for closed loops. The highest curvature occurs always at fixed nodes or in the close proximity of other dislocations. In regions of high curvature, large self-forces oc-

cur and the curvature at the segment will be near its equilibrium value. Thus, the curvature in these special locations can be determined directly from the equilibrium condition on the segment. The entire geometry of the loop is finally determined by using Eq. (4.3) at next time step.

Time step selection is determined by dislocation segment velocity and its adjacency to other segments. The time-step is selected such that, on average, dislocation-dislocation interaction is resolved within about 100 steps. If the dislocation density is ρ, the average distance between segments is on the order of $\rho^{-1/2} \sim 10^{-6} - 10^{-5}$ m. In fcc crystals, the dislocation resistivity is on the order of 5×10^{-5} Pa s, while it is about 8 orders of magnitude higher for screw segments in bcc crystals.[65] These considerations lead to a time-step of ~ 1 ns for fcc crystals and ~ 0.1 s for bcc crystals at low temperatures. When two loop segments approach each other, a short-range reaction occurs, and the time step must be reduced to determine whether the reaction will lead to annihilation or junction formation. In case of annihilation, two loops join together and form different new loops as a mode of plastic recovery. On the other hand, junction formation leads to hardening and stabilization of dislocation patterns. In either case, the minimum distance between segments on the loop itself, or on two adjacent loops is determined by calculating all local minimum distances from each node to a curved segment. By scanning all possible nodes on a loop, we obtain the minimum distance d_{min} between two loops or between two segments on the loop itself. If this value is less than two times the maximum displacement, i.e., $2d_{max}$, then the time step is adjusted to $0.25 d_{min}/d_{max}$. This procedure is repeated until loop annihilation or junction formation is completed. After annihilation or junction formation is completed, the time step is gradually increased to its maximum assigned value, as discussed above. During short-range encounters, local dislocation segment velocity can approach the sound speed, and inertial effects may have to be accounted for, if one is interested in the exact details of the short-range reaction.[48]

If new loops are generated during the short-range reaction, all nodes on the loop are rearranged. For loop junction formation, new loops are not generated, and the nodes are ordered to allow formation of straight junction segments. However, five possible cases for generating new loops are considered during segment annihilation. On the glide plane, a full dislocation loop may be totally closed, or may have closure on other glide plane via sessile threading arms formed by cross slip. Thus, we may have one of the following possibilities: (1) annihilation of two segments on the same open loop to produce one new open loop and one new closed loop; (2) annihilation of two segments on the same closed loop to produce two new closed loops; (3) annihilation of two segments on two different open-loops to produce two new open loops; (4) annihilation of two segments, one an open loop and the other on a closed one to produce one new open loop; (5) annihilation of two segments on two different closed loops to produce one new closed loop. In each case, the nodes on generated loops are reordered.

V. APPLICATIONS OF PARAMETRIC DISLOCATION DYNAMICS

A. Illustrative example: Initial bow-out of a pinned dislocation

To illustrate the computational procedure involved in the present method, we consider here a very simple example,

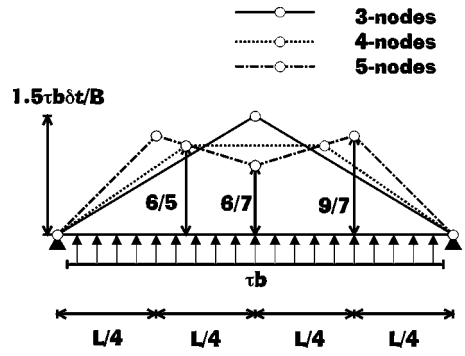

FIG. 2. Nodal displacements for the first time-step of an initially straight segment.

where the equations of motion can be solved analytically for just one time step. Our purpose here is to highlight the essential features of the present computational method. Assume that we are interested in determining the shape of a dislocation line, pinned at two ends and under the influence of pure shear loading on its glide plane. The glide mobility is assumed to be isotropic and constant, and the segments will be taken as linear for illustrative purposes only. The dislocation line is pinned at points *L* and *R*, with only two linear and equal segments connected at point *A*, as shown in Fig. 2. We will compute the shape of the line, advancing it from its initial straight configuration to a curved position. Under these simplifications, the variation in Gibbs free energy, δG for any one of the two segments is given by

$$\delta G = -B \int_0^1 V \delta r |d\mathbf{s}| = -\int_0^1 f^t \delta r |d\mathbf{s}|. \tag{5.1}$$

Now, we expand the virtual displacement and velocity in only two shape functions: $\mathcal{C}_1 = u, \quad \mathcal{C}_2 = 1-u$. Thus, $\delta r_k = \delta q_{ik} \mathcal{C}_i$, and $V_k = q_{ik,t} \mathcal{C}_i$. Since we allow the displacement to be only in a direction normal to the dislocation line (*y* direction), we drop the subscript *k* as well. For arbitrary variations of δq_{ik}, the following equation is applicable to any of the two segments (LA, AR),

$$-\int_0^1 \Delta t (f_{PK} + f_S) \mathcal{C}_i |ds| = -B \int_0^1 \Delta q_m \mathcal{C}_m \mathcal{C}_i |ds|. \tag{5.2}$$

Equation (5.2) can be explicitly integrated over a short time interval Δt. The *resistivity matrix* elements are defined by: $\gamma_{im} \equiv B \int_0^1 \mathcal{C}_i \mathcal{C}_m |\mathbf{ds}|$, and the *force vector* elements by $f_i \equiv \int_0^1 \mathcal{C}_i (f_{PK} + f_S) |\mathbf{ds}|$. With these definitions, we have the following (2×2) algebraic system for each of the two elements:

$$\Delta q_m \gamma_{im} = f_i \times \Delta t. \tag{5.3}$$

For any one linear element, the line equation can be determined by

$$[x \quad y] = \begin{bmatrix} u & 0 \\ 0 & (1-u) \end{bmatrix} \begin{Bmatrix} q_1 \\ q_2 \end{Bmatrix}. \tag{5.4}$$

And the resistivity matrix can the be simplified as

$$[\gamma_{mn}]=\frac{Bl}{6}\begin{bmatrix}2 & 1\\ 1 & 2\end{bmatrix}.$$

Furthermore, as a result of the shear stress τ and the absence of self-forces during the first time step only, the distributed applied force vector reads

$$\{f_m\}=\frac{\tau bl}{2}\begin{Bmatrix}1\\ 1\end{Bmatrix}.$$

Since the dislocation line is divided into two equal segments, we can now assemble the force vector, resistivity matrix, and displacement vector in the global coordinates, and arrive at the following equation for the global nodal displacements ΔQ_i:

$$\frac{Bl}{12}\begin{bmatrix}2 & 1 & 0\\ 1 & 4 & 1\\ 0 & 1 & 2\end{bmatrix}\begin{Bmatrix}\Delta Q_1\\ \Delta Q_2\\ \Delta Q_3\end{Bmatrix}=\frac{\tau bl\Delta t}{4}\begin{Bmatrix}1\\ 2\\ 1\end{Bmatrix}+\Delta t\begin{Bmatrix}F_1\\ 0\\ F_3\end{Bmatrix}. \tag{5.5}$$

An important point to note here is that at the two fixed ends, we know the boundary conditions, but the reaction forces needed to satisfy overall equilibrium are unknown. These reactions act on the fixed obstacles at L and R, and are important in determining the overall stability of the configuration (e.g., if they exceed a critical value, the obstacle is destroyed, and the line is released). If $\Delta Q_1=\Delta Q_3=0$ at both fixed ends, we can easily solve for the nodal displacement $\Delta Q_2=3/2(\tau b\Delta t/B)$ and for the unknown reaction forces at the two ends: $F_1=F_3=-\frac{1}{8}\tau bl$. If we divide the dislocation line into more equal segments, the size of the matrix equation expands, but nodal displacements and reaction forces can be calculated similarly. Results of analytical solutions for successively larger number of nodes on the dislocation segment are shown in Fig. 2.

B. Dislocation loop generation

Generation of new dislocation loops is an important process in determining the rate of hardening in materials under deformation. The basic mechanism involves the propagation of a dislocation segment from two immobile (fixed) ends under the action of applied stress. If the applied stress exceeds the resistance offered by the self-force, lattice friction, and additional forces from nearby dislocations, the segment length will increase. In fcc metals, the Peierls (friction) stress is very small, on the order of $10^{-5}\mu$, and is thus lower than typical applied stresses of $10^{-3}\mu$. Dislocation mobility is isotropic at all relevant temperatures because of the low value of Peierls stress in comparison to applied and self stresses on dislocation segments. Thus, the influence of the underlying crystal structure on dislocation generation is not pronounced. On the other hand, high anisotropic Peierls stresses in both fcc and diamond cubic materials (e.g., Si) imposes constraints on the shapes of generated dislocation loops in these systems, as discussed next.

1. Isotropic mobility of screw and edge segments

Figure 3 shows the results of shape computations for the Frank-Read source in a bcc crystal at high temperature,

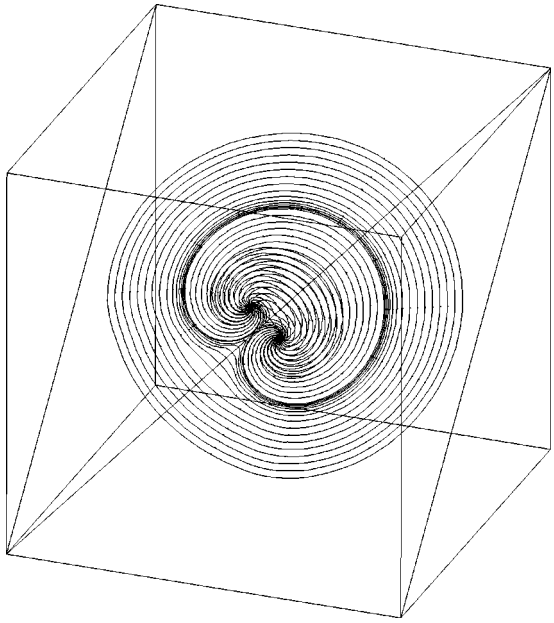

FIG. 3. Operation of the Frank-Read source for isotropic dislocation mobility on the glide plane.

where the dislocation segment mobility can be assumed to be isotropic on the $\langle 110\rangle$ glide plane. In this simulation, we use composite quintic spline segments to construct the loop after each time-step computation of the nodal displacement and tangent angle. The loop starts from an edge line segment with two fixed ends normal to the $\langle 11\bar{1}\rangle$ direction, for which we assign only three nodes at the first time step. The tangent vectors at the two end nodes are those of circular arcs constructed from three adjacent nodes. When the loop expands, more nodes are added around the two fixed end nodes (high curvature regions), while the number of nodes is automatically reduced in the low curvature region of the loop. After each time-step, the minimum distance between loop segments is calculated. If the minimum distance is detected to be less than $6|\mathbf{b}|$, and $\cos^{-1}(\mathbf{t}_1\cdot\mathbf{t}_2)=(1\pm 0.05)\pi$, the two segments are annihilated. Here, $\mathbf{t}_1$ and $\mathbf{t}_2$ are the tangent vectors for segments 1 and 2, respectively. The value of $6|\mathbf{b}|$ for the critical annihilation distance in fcc is taken from experimental measurements on Cu (Ref. 66) and Ni (Ref. 67). Results of calculations are shown in Fig. 3, where nodal positions are indicated on each loop. Details of node rearrangement before and after an annihilation reaction between two curved segments on the Frank-Read source are shown in Fig. 4.

The influence of the self-force on dislocation motion is significant, especially during short-range interaction of dislocation segments. In Fig. 5, the angular distribution of the self-force on the glide dislocation loop, immediately after its formation by annihilation of opposite segments on the original dislocation line is shown. It is clear that the distribution of the self-force is negative everywhere on the loop, except for the small range of angles surrounding the newly formed dislocation segment. In this region, the self-force is positive, and thus it will assist the applied stress in expanding this curved region faster than others on subsequent time-steps. The action of applied and self-forces tend to even out curvature variations on the entire loop, once the short-range reac-

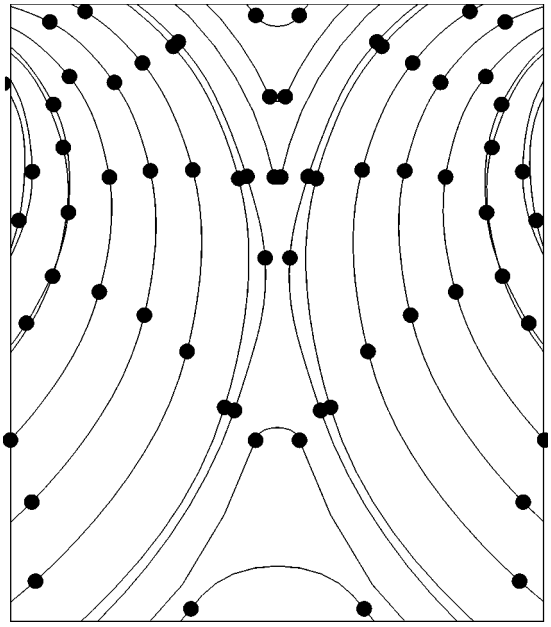

FIG. 4. Details of nodal arrangements before annihilation of opposite-character segments.

tion is completed. The self-force is seen to be higher for the screw segments at $\theta = 90°$ and 270°, as compared to segments with a pure edge character.

2. bcc metals at low temperature

In bcc metals, the primary slip system is $\{110\}\langle 111\rangle$, although slip on secondary $\{112\}$ and $\{123\}$ planes are possible.[46] Slip trace analysis at low temperature[68,69] indicates that the main slip planes are $\{110\}$, and that dislocations are either of the screw or edge type. At temperatures below $T_a \sim 0.15 T_m$, dislocations in bcc metals tend to move as straight lines, indicating that the mobility of the edge component is extremely high.[65] The mobility of screw segments is controlled by double kink nucleation below the *athermal* temperature, T_a. Peierls lattice friction stress on screw components is very high, and the corresponding mobility is low. As the temperature increases, the influence of lattice friction on screw component mobility is reduced, and the mobility of screw and edge dislocations become comparable. It is expected, therefore, that dislocations become very straight at low temperatures, and that significant curvatures develop at higher temperatures. To adequately represent this physical picture, we use composite cubic spline curves joined with linear segments when necessary, and still maintain C^2 continuity at all nodes. In this case, the tangent directions of each curved segment are predetermined by crystallography (i.e., $\langle 111\rangle$ directions for screw components), and only the magnitude of the tangent vector needs to be calculated from the condition of continuity. Additionally, nodes on expanding loops in this case are not redistributed, but are selected to ensure construction of polygonal loop shapes, as is experimentally observed at low temperature.[69] The construction procedure of polygonal loop geometry is described as follows.

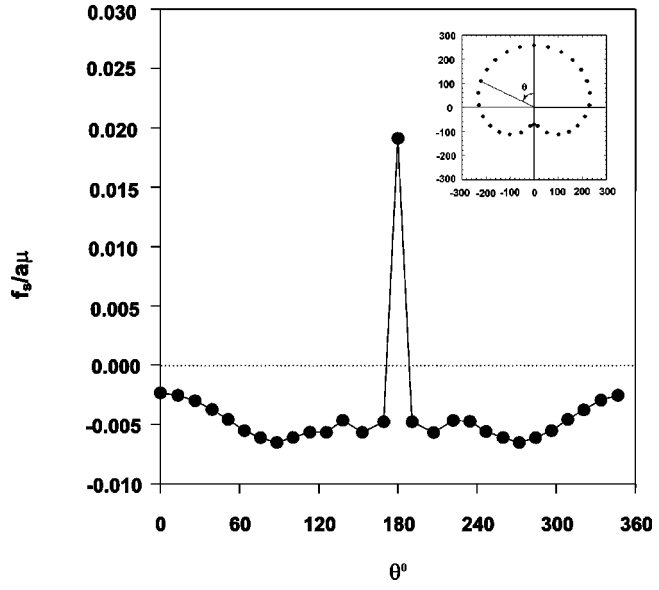

FIG. 5. Angular variation of the self force (units of $\sigma/\mu a$) in copper for the Frank-Read source after segment annihilation. The angle θ is defined in the insert. All distances on the figure are in units of the lattice constant.

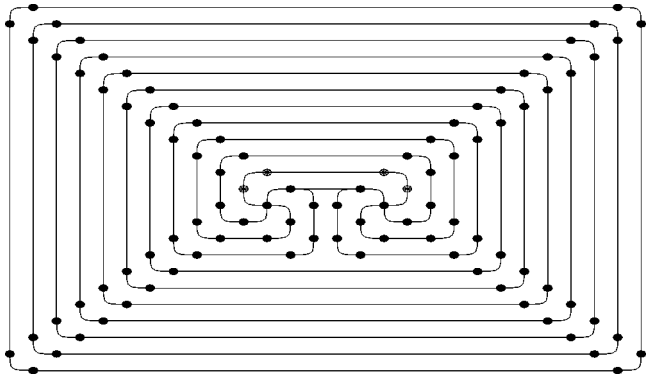

FIG. 6. Double-ended Frank-Read source in bcc metals. The straight segments are either screw or edge, while the curved corners are of mixed type.

First, straight linear segments are assigned parallel to specific crystallographic directions (i.e., $\langle 111\rangle$) for screw components. The displacement is computed for the entire linear segment in the normal edge direction. Then, two adjacent nodes at each corner of a the resulting rectangle are assigned, such that the distance of each node from the corner is proportional to the magnitude of the displacement, which is determined by the anisotropic mobility. Finally, after nodes are generated, the tangent direction of each node is aligned with the side of the polygon or is assigned a prescribed angle with the polygonal direction as an additional degree of freedom. For example, if the temperature is increased in bcc crystals, slight curvatures can be expected, and the tangent magnitudes can be solved for by applying the condition of C^2 continuity. It is noted that at very low temperatures in bcc metals, the mobility of edge components (kinks) is much higher than that of screw segments, and thus dislocation lines will be predominantly of the screw type. These features of adaptive shape computations are illustrated in Fig. 6 for low temperature and Fig. 7 for higher temperatures.

3. Dislocation sources in Si

Motion of dislocations on the glide plane of dc crystals, such as Si, occurs by breaking and reconstruction of strong

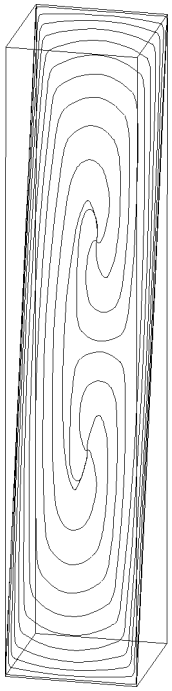

FIG. 7. Dislocation loop generation by the Frank-Read mechanism for anisotropic mobility of screw and edge components.

covalent bonds. Thus, the resistance of the lattice to dislocation motion is significant up to very high temperatures (e.g., 1200 K in Si). The dislocation must overcome a large energy barrier in the direction of maximum bond strength (i.e., the three $\langle 110 \rangle$ close-packed directions on the $\{111\}$ family of slip planes), and a smaller one in directions $\pm 60°$ to those primary ones. Dislocation segment mobility in Si is rather low, which leads to a time step on the order of 0.01 s, similar to the situation in bcc metals.[70]

When general cubic spline segments are used, we must solve for tangent vectors at each node, in addition to nodal displacements in order to generate the dislocation loop geometry at successive time steps. However, for special polygonal loop geometries, additional constraints are needed to maintain accurate loop profiles. For this purpose, we use two types of segments: linear ones for the sides and curved segments for polygonal corners. The curvature of all nodes is thus constrained to be zero, which guarantees the alignment of polygonal sides to crystallographic directions, as can be seen in Fig. 8. The procedure outlined above produces hexagonal loops with rounded corners, in agreement with the experimental observations on dislocation sources in Si by Dash.[71]

C. Dislocation loop interactions

In Fig. 9, two initial screw segments of equal length are assumed to be collinear, and of the same initial length on the $[110]$-slip plane of a bcc crystal at high temperature, and a high shear stress is applied on the slip plane. Bowing of the two segments is tracked with nodal displacements and tangent vector direction, and the loops are reconstructed by quintic spline segments after each time-step. The process is repeated until any two curved segments on the same loop, or on the two different loops, approach each other. The annihilation criterion is applied, leading to the loop profiles shown in Fig. 9. The applied stress is higher than the maximum value of the self energy after the two loops join one another, because the nodal curvatures are much smaller than corresponding values near the fixed ends of the each loop. Hence, further nodal displacements are not influenced as much with nodal curvatures, once the two loops join together as a single loop. Another illustration of loop-loop interaction is shown in Fig. 10, where two glide loops on different $\{111\}$ planes interact and form a sessile junction at the intersection between the two glide planes. In this case, the Burgers vector of the resulting junction does not lie on any of the two slip planes.

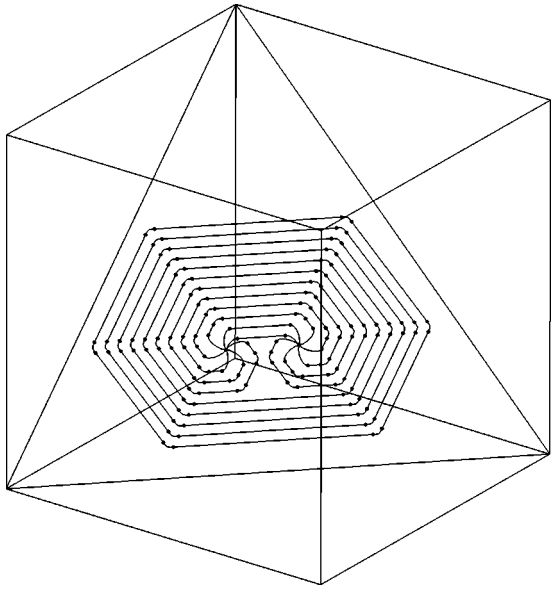

FIG. 8. Dislocation generation in covalently bonded silicon. The directions of the hexagon sides are along $\langle 111 \rangle$ orientations for screw segments, and $\pm 60°$ for mixed ones.

VI. SUMMARY AND CONCLUSIONS

In a previous paper,[54] we presented a computational method for accurate calculation of the isotropic elastic field of arbitrary-shape dislocation loops. The main motivation behind this work was to enable calculations of thermodynamic forces on dislocation segments in deforming materials. This task has been addressed in the present work, where we developed a variational method, which can be utilized to derive the equations of motion of arbitrary-shape dislocation loops in complex 3D geometry. The present method is in the

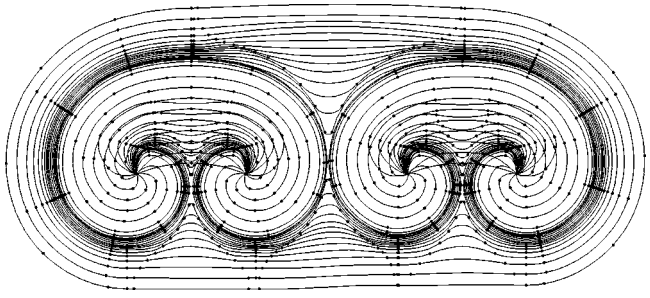

FIG. 9. Coplanar dislocation loop interaction.

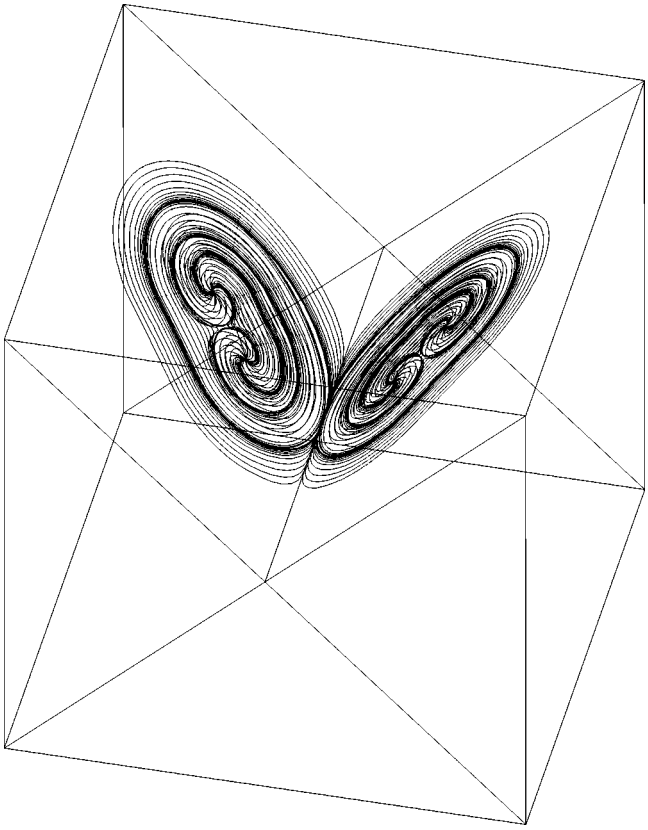

FIG. 10. Formation of a dislocation junction in bcc metals.

spirit of the finite element method in structural mechanics, where the dislocation line is segmented and described by known shape functions in a linear combination of unknown generalized coordinates, such as position, tangent, and normal vectors. Physical arguments are used to ascribe constraints on these generalized coordinates, and thus reduce the number of equations of motion. The method is illustrated in a number of applications on dislocation loop generation and interactions in bcc, fcc, and dc materials. Many applications of the present method are feasible, especially in areas where continuum descriptions of plastic deformation fall short. One such application is the simulation of the onset of plastic instabilities and the formation of dislocation channels in irradiated materials.[72,73] It is concluded that the present method offers a number of potential advantages.

(1) The method provides a general and natural description of dislocation loop geometry that is not determined by an underlying computational mesh, and which easily conforms to physical constraints imposed by the crystal structure.

(2) Numerical force divergence problems for very short straight segments are totally avoided. Force computations are also accurate for long segments as well. The moments of the total force distribution function are determined by sampling from positions on the entire segment.

(3) The method is accurate in rather complex situations involving high curvature regions, strongly interacting dislocations, cross slip, strong pinning, etc.

(4) Various segment types can be easily mixed within the same computation, thus leading to a reduction in the overall computational burden.

(5) Since the final equation is of a matrix form for the DOF's, the method is automatically compatible with the standard finite element technique. It is thus natural to directly couple the present formulation with the computational methods of continuum mechanics.

(6) The computational speed of stress, force, and energy calculations per segment is comparable to purely analytical solutions of straight segments.[53] One of the main advantages of the present method is the possibility of reducing the number of necessary segments by two orders of magnitude (in fcc simulations, for example), and hence the number of interactions by four orders of magnitude.

ACKNOWLEDGMENTS

The authors would like to acknowledge the financial support of the U.S. Department of Energy/Office of Fusion Energy through Grant No. DE-FG03-98ER54500, and Lawrence Livermore National Laboratory through Grant Nos. B339029, MI-98-031, and MI-99-017, with UCLA. The support and encouragement of Dr. T. de la Rubia, Dr. D. Lassila, and Dr. W. King of LLNL are gratefully recognized. Numerous discussions with Professor J. Hirth and Professor H. Zbib, and with Dr. K. Schwarz, Dr. L. Kubin, and Dr. B. Devincre have been illuminating.

[1] R. J. Amodeo and N. M. Ghoniem, Res. Mech. **23**, 137 (1988).
[2] H. Mughrabi, Acta Metall. **31**, 1367 (1983).
[3] H. Mughrabi, Mater. Sci. Eng. **85**, 15 (1987).
[4] L. P. Kubin, in *Treatises in Materials Science and Technology*, edited by R. W. Cahn *et al.* (Chemie, Weinhum, Germany, 1993).
[5] J. Kratochvil and M. Saxlova, Solid State Phenom. **23/24**, 369 (1992).
[6] G. Ananthakrishna, Solid State Phenom. **23/24**, 417 (1992).
[7] G. Ananthakrishna, C. Fressengeas, M. Grosbras, J. Vergnol, C. Engelke, C. Plessing, H. Neuhauser, E. Bouchaud, J. Planes, and L. P. Kubin, Scr. Metall. Mater. **32**, 1731 (1995).
[8] M. Zaiser, M. Avlonitis, and E. C. Aifantis, Acta Mater. **46**, 4143 (1998).
[9] P. Hahner, K. Bay, and M. Zaiser, Phys. Rev. Lett. **81**, 2470 (1998).
[10] V. Gregor and J. Kratochvil, Int. J. Plast. **14**, 159 (1998).
[11] U. F. Kocks, A. S. Argon, and M. M. Ashby, in *Progress in Materials Science*, edited by B. Chalmers, J. W. Christian, and T. B. Massaiski (Pergamon Press, Oxford, 1975), Vol. 19, p. 1.
[12] N. M. Ghoniem, J. R. Matthews, and R. J. Amodeo, Res. Mech. **29**, 197 (1990).
[13] D. Walgraef and E. Aifantis, J. Appl. Phys. **58**, 688 (1985).
[14] D. Holt, J. Appl. Phys. **41**, 3197 (1970).
[15] J. Lepinoux and L. P. Kubin, Scr. Metall. **21**, 833 (1987).
[16] N. M. Ghoniem and R. Amodeo, Solid State Phenom. **3&4**, 377 (1988).
[17] A. N. Guluoglu, D. J. Srolovitz, R. LeSar, and R. S. Lomdahl, Scr. Metall. **23**, 1347 (1989).

[18] N. M. Ghoniem and R. J. Amodeo, in *Patterns, Defects and Material Instabilities*, edited by D. Walgreaf and N. M. Ghoniem (Kluwer, Dordrecht, 1990), p. 303.
[19] R. J. Amodeo and N. M. Ghoniem, Phys. Rev. B **41**, 6958 (1990).
[20] R. J. Amodeo and N. M. Ghoniem, Phys. Rev. B **41**, 6968 (1990).
[21] R. J. Amodeo and N. M. Ghoniem, in *Modeling of Deformation of Crystalline Solids*, edited by T. Lowe, T. Rollett, P. Follansbee, and G. Daehn (TMS Press, Warrendale, PA, 1991), p. 125.
[22] I. Groma and G. S. Pawley, Philos. Mag. A **67**, 1459 (1993).
[23] V. A. Lubarda, I. A. Blume, and A. Needleman, Acta Metall. Mater. **41**, 625 (1993).
[24] H. Y. Wang and R. Lesar, Philos. Mag. A **71**, 149 (1995).
[25] D. B. Barts and A. E. Carlsson, Phys. Rev. E **52**, 3195 (1995).
[26] H. Cleveringa, E. van der Giessen, and A. Needleman, J. Phys. IV **8**, 83 (1998).
[27] D. Raabe, Philos. Mag. A **77**, 751 (1998).
[28] L.P. Kubin, G. Canova, M. Condat, B. Devincre, V. Pontikis, and Y. Brechet, Solid State Phenom. **23/24**, 445 (1992).
[29] B. Devincre and M. Condat, Acta Metall. Mater. **40**, 2629 (1992).
[30] B. Devinere, V. Pontikis, Y. Brechet, G. Canova, M. Condat, and L. P. Kubin, in *Microscopic Simulations of Complex Hydrodynamic Phenomena*, edited by M. Mareschal and B. L. Lolian (Plenum Press, New York, 1992), p. 413.
[31] G. Canova, Y. Brechet, and L. P. Kubin, in *Proceedings of the 13th Risø Internationl Symposium on Materials Sciience*, edited by S. I. Anderson *et al.* (Risø National Laboratory, Roskilde, Denmark, 1992).
[32] L. P. Kubin and G. Canova, Scr. Metall. Mater. **27**, 957 (1992).
[33] L. P. Kubin, Phys. Status Solidi A **135**, 433 (1993).
[34] G. Canova, Y. Brechet, L. P. Kubin, B. Devincre, V. Pontikis, and M. Condat, *Microstructures and Physical Properties*, edited by J. Rabiet (CH-Transtech, 1993).
[35] B. Devincre and L. P. Kubin, Modell. Simul. Mater. Sci. Eng. **2**, 559 (1994).
[36] B. Devincre, in *Computer Simulation in Materials Science*, edited by H. O. Krichner *et al.* (Kluwer Academic Press, Dordrecht, 1996), p. 309.
[37] B. Devincre and L. Kubin, Philos. Trans. R. Soc. London, Ser. A **355**, 2003 (1997).
[38] A. M. Moulin, P. Condat, and L. Kubin, Acta Mater. **45**, 2339 (1997).
[39] J. P. Hirth, M. Rhee, and H. Zbib, J. Comput.-Aided Mater. Des. **3**, 164 (1996).
[40] K. W. Schwarz and J. Tersoff, Appl. Phys. Lett. **69**, 1220 (1996).
[41] K. W. Schwarz, Phys. Rev. Lett. **78**, 4785 (1997).
[42] K. W. Schwarz and F. K. LeGoues, Phys. Rev. Lett. **79**, 1877 (1997).
[43] H. M. Zbib, M. Rhee, and J. P. Hirth, Int. J. Mech. Sci. **40**, 113 (1998).
[44] D. C. Chrzan and M. S. Daw, Phys. Rev. B **55**, 798 (1997).
[45] L. M. Brown, Philos. Mag. **15**, 363 (1967).
[46] J. P. Hirth and J. Lothe, *Theory of Dislocations*, 2nd ed. (McGraw-Hill, New York, 1982).
[47] W. G. Johnston and J. J. Gilman, J. Appl. Phys. **30**, 129 (1959).
[48] H. Huang, N. M. Ghoniem, T. Diaz de la Rubia, M. Rhee, H. Zbib, and J. Hirth, J. Eng. Mater. Technol. **121**, 143 (1999).
[49] A. C. Erringen, *Mechanics of Continua* (Wiley, New York, 1967), p. 127.
[50] L. E. Malvern, *Introduction to the Mechanics of a Continuous Medium* (Prentice-Hall, Englwood Cliffs, NJ, 1969).
[51] M. O. Peach and J. S. Koehler, Phys. Rev. **80**, 436 (1950).
[52] N. M. Ghoniem and M. Bacaloni (unpublished).
[53] N. M. Ghoniem, J. Eng. Mater. Technol. **121**, 136 (1999).
[54] N. M. Ghoniem and L. Z. Sun, Phys. Rev. B **60**, 128 (1999).
[55] S. D. Gavazza and D. M. Barnett, J. Mech. Phys. Solids **24**, 171 (1976).
[56] R. deWit, Solid State Phys. **10**, 269 (1960).
[57] L. A. Gore, Ph.D. thesis, Stanford University, 1980.
[58] J. Lothe and J. P. Hirth, J. Appl. Phys. **38**, 845 (1967).
[59] G. Nicolis and I. Prigogine, *Self-Organization in Nonequilibrium Systems* (Wiley, New York, 1977).
[60] L. Onsager, Phys. Rev. **37**, 405 (1931).
[61] D. Maroudus, Appl. Phys. Lett. **67**, 798 (1995).
[62] Z. Suo, Adv. Appl. Mech. **33**, 1 (1996).
[63] T. J. R. Hughes, in *Computational Methods for Transient Analysis*, edited by T. Belytschko and T. J. R. Hughes (North-Holland, Amsterdam, 1983), p. 67.
[64] R. Sedlaček, Philos. Mag. Lett. **76**, 275 (1997).
[65] L. P. Kubin, B. Devincre, and M. Tang, J. Comput.-Aided Mater. Des. **5**, 31 (1998).
[66] U. Essmann and H. Mughrabi, Philos. Mag. A **40**, 731 (1979).
[67] B. Tippelt, J. Bretschneider, and C. Holste, Philos. Mag. Lett. **3**, 161 (1996).
[68] S. Takeuchi and K. Maeda, Acta Metall. **25**, 1485 (1977).
[69] W. Wasserbach, Philos. Mag. A **53**, 335 (1986).
[70] A. Moulin, M. Condat, and L. P. Kubin (unpublished).
[71] W. C. Dash, J. Appl. Phys. **27**, 1193 (1956).
[72] N. M. Ghoniem and B. Singh, in *Proceedings of 20th Risø International Symposium on Materials Science*, edited by J. B. Bilde-Sørensen *et al.* (Roskilde, Denmark, 1999).
[73] N. M. Ghoniem, B. Singh, L. Z. Sun, and S.-H. Tong (unpublished).